IN-PLANE PERMEABILITY OF ORIENTED STRAND LUMBER. PART II: MICROSCOPIC INVESTIGATION OF VOID STRUCTURE DURING COMPRESSION

Chao Zhang
Graduate Research Assistant

*Gregory D. Smith**†
Associate Professor
Department Of Wood Science
University Of British Columbia
Vancouver, BC, Canada V6T 1Z4

(Received June 2009)

Abstract. This study investigated the changes of void structure in oriented strand lumber samples pressed to different densities using microscopic techniques. Specimens of five densities, 450, 550, 625, 700, and 800 kg/m^3, were examined. A method for preparing a large sectional area of wood composites for examination in a light microscope was developed. It was able to retain the original void structure and to provide high-quality images for further investigation. Microscope slides mounted with thin cross-sections for each density were prepared and then examined using fluorescence microscopy. The size and quantity of interstrand voids decreased dramatically with increasing board density. The forming and deformation of interstrand and intrastrand (ie cell lumens) voids, including failure of cell walls and nonhomogeneous collapse of cells, were observed. Generally the vessels were compressed before fibers as a result of their difference in diameter and cell wall thickness. The variability of deformation between regions within a strand and between strands within a mat was high, due to differences in strand cutting orientation, heterogeneity of mat structure, and strand property variation created by its source in different positions on a tree stem and between trees.

Keywords: Strands, wood composites, microscopic, voids, compression, vessel, fiber.

INTRODUCTION

Hot-pressing is one of the most important processes in the manufacture of strand-based wood composites. The mechanical compression of a loosely formed mat leads to the closure of voids between strands and the viscoelastic deformation of strands, which becomes permanent after the resin cures. The deformation of strands is accompanied by the collapse of cell walls and compression of cell lumens. As a porous material, most properties of strand-based wood composites, including the strength, thickness swelling, elasticity, etc, are affected by the void structure. Specific permeability is a measure of the ease with which a fluid flows through a material (Siau 1995) and is dependent on the void size distribution and their connectivity. Therefore, the investigation of the changes in microscopic structure of voids during compression should provide insight into the mechanism of flow in a strand mat.

Since the 1970s, microscopic and advanced imaging techniques such as high-magnification light microscopy, scanning electron microscopy (SEM), and X-ray tomography have been used to study the structure of porous materials, eg concrete, soil, and rocks (Flannery et al 1987; Blair et al 1996; Schaap and Lebron 2001; Lu et al 2006). These microscopic techniques also have been used to characterize the properties of wood materials.

Kultikova (1999) evaluated the effect of densification on the structure of yellow-poplar and loblolly pine; a considerable difference between

* Corresponding author: Greg.Smith@ubc.ca
† SWST member

earlywood and latewood was found in pine under compression, whereas the compression distribution in poplar was more uniform. A series of investigations by Tabarsa and Chui (2000, 2001) studied the microscopic behavior of several different wood species under radial compression. They found that cell wall collapse was limited to the earlywood cells for white spruce and jack pine, whereas deformation was dominated by vessel collapse in white ash and aspen. Müller et al (2003) used SEM to investigate the cell deformation of several wood species loaded perpendicular to the grain. The deformation mode varied significantly and ranged from ductile-plastic deformation in spruce, to elastomeric yielding in beech, to brittle fracture in oak. Geimer et al (1985) were the first to microscopically examine cellular damage within Douglas-fir flakeboard under transverse compression. It was found that cellular structural damage was due to a combination of buckling, shearing, and bending failure of cell walls in the earlywood zones of strands that were compressed by the latewood areas on adjacent flakes. Several research groups have used X-ray tomography in an attempt to quantify the void geometry of wood composites. Sugimori and Lam (1999) developed a method to analyze the macrovoid distribution in strand-based wood composites. The X-ray images were converted to a 3D measurement of the macrovoids. Zhang et al (2005) provided 2D and 3D visualizations of intervoid structures in oriented strandboard (OSB) and found that voids decreased exponentially with increasing mat density.

To date, there is limited information on the microscopic structural changes in strand-based wood composites during compression. This study aims to examine the inter- and intrastrand voids of oriented strand lumber (OSL) at different densities using microscopic techniques and to investigate the void development. As discussed in Part I (Zhang and Smith 2010), gas flows through strand-based panels via two types of voids: interstrand and intrastrand voids (Dai and Steiner 1993). The hypothesis made by Bolton and Humphrey (1994) that gas flow occurred predominantly through interstrand voids was validated by Dai et al (2005) for the transverse permeability in OSB. The other objective of this work was to test the validity of this hypothesis for in-plane permeability by investigating the size of inter- and intrastrand voids at different levels of densification.

MATERIALS AND METHODS

The OSL specimens were obtained from the boards made for in-plane permeability measurements in Part I (Zhang and Smith 2010). Microscopic sections were taken in the cross-section perpendicular to the strand alignment direction as shown schematically in Fig 1. The images of macrovoids were obtained by a handheld digital camera. Traditional methods of preparing slides for microscopic examination, eg sledge microtome and razor blade, did not work because the thin sections sliced by the microtome or blade were brittle and easily broken leaving the sections so damaged that the voids in them did not correspond to the true state of voids in the original sample. Epoxy impregnation of the specimen was tried and it retained the integrity of the internal structure but made the samples too hard to be cut with a microtome blade. A method to prepare slides was finally developed based on the techniques reported by Jana (2006). The procedure was as follows:

1. Four specimens were randomly selected from each density and two slides prepared for each specimen. The samples, 50.8-mm long and 25.4-mm wide, were cut from the boards (31.8-mm thick) and oven-dried until a constant weight was achieved.

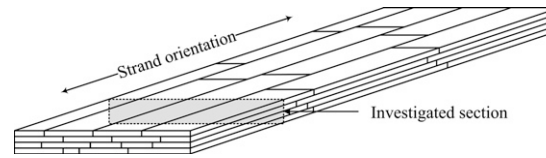

Figure 1. The location and orientation of the microscopically investigated sections within in a panel.

2. A surface was prepared by hand sanding with a series of finer and finer sandpapers: 80, 120, 180, 220, 330, 400, 800, and finally 4000 grit. When the dust accumulated, it was blown away by high-pressure air (about 250 kPa), the purpose of which was to ensure a clean surface to bond with the glass slide.
3. The prepared surface was bonded to a glass microscopy slide with hot-melt adhesive (Scotch-Weld^{TM} 3738AE with an adhesive failing point 54°C and a melting point 86°C). The slide was heated to about 70°C on a hot plate to achieve a thin, relatively uniform layer of hot melt adhesive on it. The section was pressed down onto the molten adhesive and removed from the hot plate to set the adhesive, as shown in Fig 2a.
4. The glass slide with a thick sample section, 3-4 mm, was carefully cut off with a hand saw, as shown in Fig 2b.
5. The thick section was hand sanded to a thickness of less than 200 μm using 80-, 120- and 180-grit abrasive papers and then polished with successively finer abrasive papers of 220, 330, 400, 800, and 4000 grit until a high-quality, damage-free surface was obtained. Like in Step 2, the dust was blown away with pressurized air to prevent coarser dust remaining on the surface. The finished slides are shown in Fig 2c.

This method is a dry process requiring no solvent and maintains the original void states. A full cross-section through the board thickness (approximately 25 × 32 mm) could be examined on one slide, but this technique was time-consuming requiring about 3 h per slide. The slides were then examined using a JENAMED 2 fluorescence microscope, to which a Lumenera Infinity 3 camera was connected to capture the images. More than 150 images were recorded from 8 randomly chosen cross-sections for each density. All the microscopic images in this article (eg Fig 3b) are shown with the horizontal width of each section corresponding to the thickness of the original panels.

Figure 2. Slide preparation processes: (a) samples bonded to glass slide, (b) thick sections cut off with slides, and (c) finished slides after sanding.

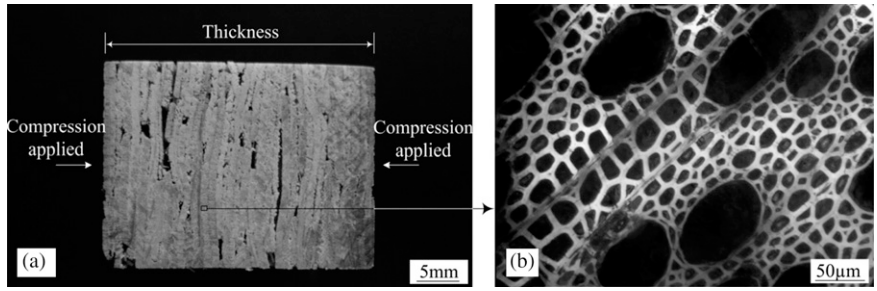

Figure 3. Orientation of images: (a) the location of an image on a cross–section; (b) the image obtained from a microscope (450 kg/m^3).

RESULTS

Interstrand Voids

Close examination of a section from the 450-kg/m^3 board (Fig 4) suggests how different void shapes were formed during densification. The overlapping of strands created bridges on the side of one or more strands forming interstrand voids of a rectangular or triangular shape. The cross-section shown in Fig 4, perpendicular to strand alignment direction, is the sectional area that in-plane flow moves through. Dai et al (2005) defined the two types of voids as noncontact voids and partially filled edge voids. The only difference with this study was that Dai et al (2005) presented the voids on a cross-section parallel to the strand alignment direction. During densification, the longer and wider voids were eliminated first as the strands over these voids tended to have larger displacement than those over the shorter and narrower voids if loaded with the same compression. Therefore, noncontact voids were more frequently found in lower density samples (450 and 550 kg/m^3), whereas partially filled edge voids became more common for higher density (625 kg/m^3 or greater).

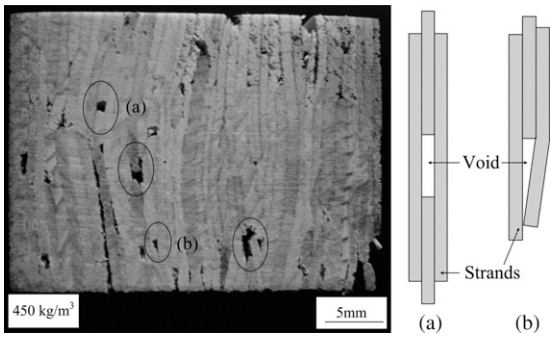

Figure 4. The formation of interstrand voids: (a) rectangular shaped void; (b) triangular shaped void.

At a magnification of ×25, interstrand voids appeared as brighter areas and strand contacts at strand boundaries as darker areas (Fig 5a-b). The voids were brighter than the strand contact zones because of the penetration of hot-melt, which easily transmitted light. When comparing the images obtained from samples of different densities, many large and continuous voids were visible in the 450-kg/m^3 samples, fewer voids and smaller voids in 550 kg/m^3, and fewer voids in 625 kg/m^3. For 700- and 800-kg/m^3 samples, only one or two per slide was observed, which indicated that the maximum contact area between the strands was reached at 625-700 kg/m^3. From the macroscopic and microscopic investigations, it was clear that the interstrand voids decreased drastically in size and quantity with increasing panel density, in agreement with the exponential decreasing of void ratio reported by Zhang et al (2005).

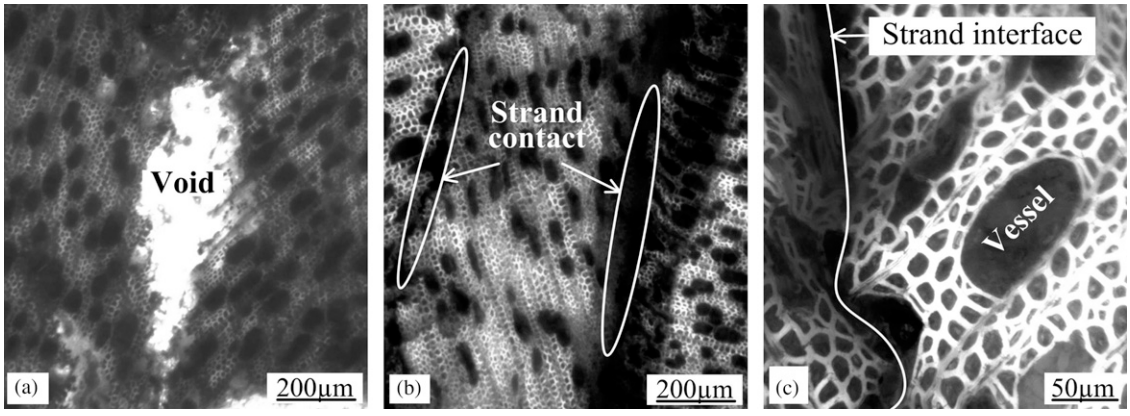

Figure 5. Sections of 625-kg/m^3 samples viewed under a microscope showing: (a) an interstrand void region that has been impregnated with hot melt glue; (b) interfacial contact areas between adjacent strands; and (c) magnified interfacial contact, indicating interstrand voids smaller than vessels.

Figure 5c shows the contacts between strands at higher magnification (×125). This kind of contact was defined as a completely filled edge void by Dai et al (2005). The image shows that the cells close to strand boundaries were more compressed than those some distance away; voids at the strand interface (interstrand) were smaller than vessel lumens inside the strands (intrastrand), suggesting that gas may preferentially flow through intrastrand voids. After analyzing more than 100 images for each density, the phenomena of interstrand voids smaller than intrastrand voids were commonly found in the specimens with a density higher than 625 kg/m^3.

Intrastrand Voids

Increasing board densification also significantly changed cell structures inside strands in terms of cell wall collapse. Cell wall failure was sometimes caused by buckling under an axial compression as shown in Fig 6a; at other times, they collapsed in a more complex manner, including shearing and bending, because of a combination of axial and lateral loads resulting from the orientation of that portion of the cell wall with respect to the loading direction as shown in Fig 6b. In both cases, cell wall collapses had drastically changed the shape and size of cell lumens. Geimer et al (1985) reported the same combination of bucking, shearing, and bending failures of cell walls in Douglas-fir flakeboard, which indicated that the three failure patterns universally occurred in strand mats regardless of if they were made from softwoods or hardwoods.

As shown in Fig 6c, vessels were found to be much easier to compress than fibers, which corresponded to what was observed by Tabarsa and Chui (2001) in an aspen cube (8 mm) under radial compression and that found by Müller et al (2003) in oak loaded perpendicular to grain. Vessels have a larger diameter and thinner cell walls than fibers making them more susceptible to compression. After investigating the state of vessels and fibers under different densification levels, the development of cell structures with an increasing compression can be generalized as follows (Zhang 2009): in those strands not compressed at low-density samples, vessels are circular or subcircular shaped; then the circular vessels becomes oval, whereas the change of fibers is not evident yet; under further compression, the curved edges of vessels become straight and the fiber deformation becomes noticeable; after that the rays start to transfer from straight lines into curves resulting in the cell arrays between them becoming distorted, meanwhile the vessels are compressed to a high length/width ratio until the width of vessels becomes close to that of the nearby fibers; finally, both vessels and fibers

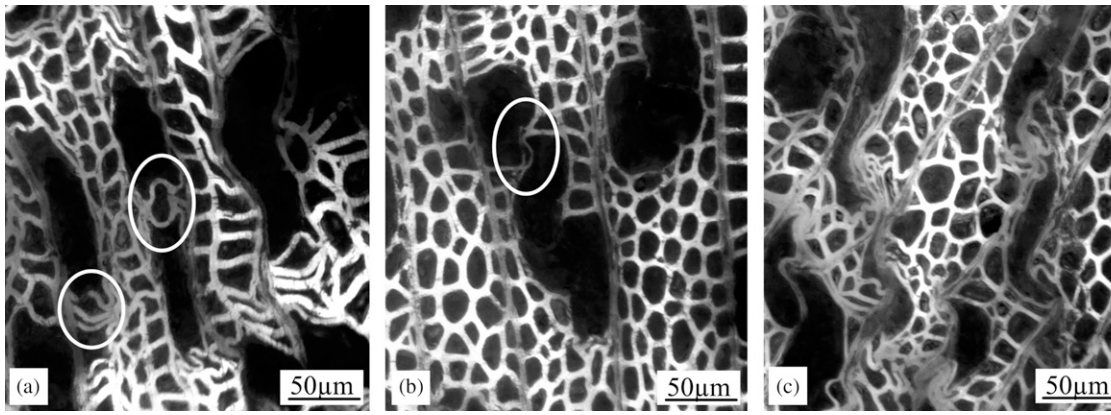

Figure 6. (a) Cell wall failure because of buckling under axial loads; (b) cell wall failure because of bending and buckling under a combination of axial and lateral loads; and (c) vessels compressed before any substantial deformation of fibers occurs.

are substantially compressed to almost the same length/width and some vessel lumens are totally closed up.

However, the behavior of aspen strands in a densified mat is more complicated and unpredictable than the previous description because of a high variability in strand property and local compressive stress state. For example, sometimes the entire row of cells fails first, whereas the nearby vessels remain relatively unchanged in shape (Fig 7a). This phenomenon has not been reported in the examination of hardwood by Tabarsa and Chui (2001) or Müller et al (2003). However, it does agree with what Geimer et al (1985) found in Douglas-fir flakeboard in where entire rows of tracheids had failed. Furthermore, even though vessels may be in close proximity to each other, they do not necessarily react simultaneously to the applied stress; as shown in Fig 7b, the two vessel lumens in the white circle collapsed first, whereas those on the left side remained intact. These results indicate that the compression applied on a strand as well as the compressive modulus/strength within a strand is very inhomogeneously distributed.

The heterogeneity of different strands within one sample is also remarkable. As shown in Fig 8, both uncompressed (Fig 8a) and highly compressed strands (Fig 8b) were present in the same 450-kg/m^3 specimen. One might expect that the less compressed strands would be located in the core area, whereas those highly compressed are closer to the surface. This was not the case after carefully examining a full cross-sectional area from top to bottom where the most compressed strands seemed to be randomly distributed. Similar patterns were also found in all other density samples and the key difference being that more of the highly

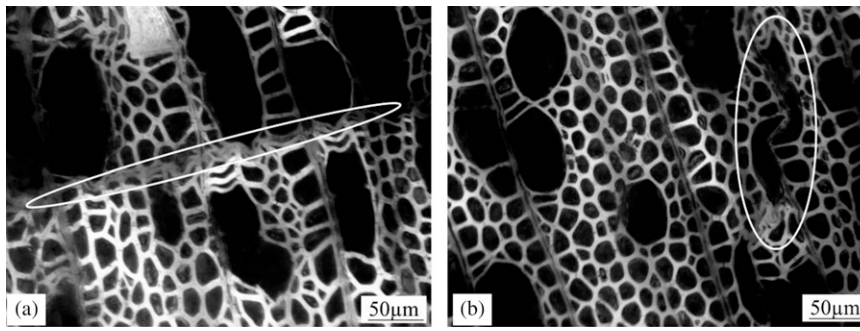

Figure 7. Nonuniform compression inside one strand: initial failure occurs (a) in one row of cells and (b) in vessel elements.

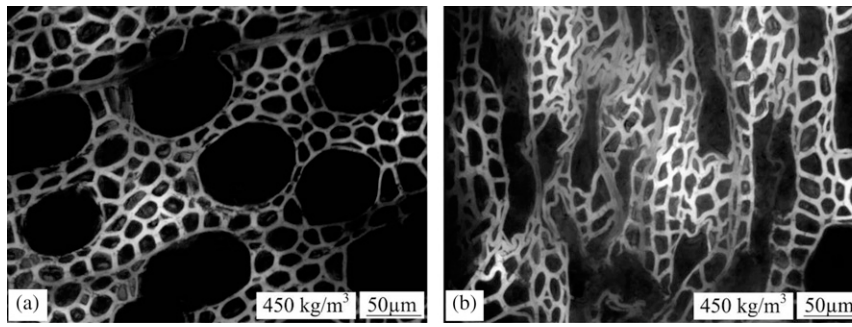

Figure 8. Different compression stages coexisting in 450-kg/m^3 samples: (a) cells at noncompressed stage and (b) highly compressed cells.

densified strands were present in higher density boards.

DISCUSSION

The investigation of interstrand voids indicated that their sizes and quantities decreased drastically during compression. For 450-, 550-, and 625-kg/m^3 specimens, interstrand voids were commonly found and had a remarkably larger size than intrastrand voids; whereas for 700 and 800 kg/m^3, the presence of interstrand voids was negligible at both macroscopic and microscopic levels in terms of their quantity as well as sizes compared with intrastrand voids. Based on this analysis, the in-plane gas flow in the OSL samples could be described as follows: in low-density panels (450 and 550 kg/m^3 boards), the flow through interstrand voids dominates; as the mat densification increases, the interstrand voids are compressed and closed up causing the gas to be forced through the intrastrand voids (at approximately 625 kg/m^3); at higher density levels (700 and 800 kg/m^3), the intrastrand voids dominate the in-plane flow. This conclusion does not agree with the hypothesis made by Bolton and Humphrey (1994) that interstrand voids controls permeability. Dai et al (2005) proved that this hypothesis was valid for transverse permeability of OSB. The results of this study do not necessarily conflict with those of Dai et al (2005) as this work focused on OSL whereas their work focused on OSB. The geometry of the voids in the in-plane direction are very different in these board types and likely explains the difference in findings.

The compression behavior of vessels and fibers was different. In the early stages of compression, vessels deformed markedly, whereas most fibers retained their original shapes; with increasing compression, both vessels and fibers began to deform simultaneously. When the cell walls fractured, the cross-sectional area through which gases can flow was greatly reduced and, from the data, results in an exponential decrease in the permeability of those samples. As shown in Figs 6, 7, and 8, the inhomogeneous behavior of cells was found between different cell types, between different regions within a strand, and between different strands in a specimen. The reasons leading to this variability include the following factors:

1. Differences in cell diameter and cell wall thickness between vessels and fibers. According to Kostiainen et al (2008), vessels in aspen had an average diameter of 51.5 μm and fibers 10.6 μm. The vessels in aspen, surrounded by thin-walled paratracheal parenchyma, were of larger diameter than fibers and were more easily collapsed than thick-walled fibers (Panshin and deZeeuw (1980).
2. The orientation of the strands. Whereas the long axis of the strand is parallel to the longitudinal direction of a wood, the cross-section could be cut from a tangential, radial, or some plane between the two as shown in Fig 9; the dotted lines in the samples section schematics indicate the direction of the rays. Figure 10 shows a magnified view of strands in these three orientations. Generally, when the strands are compressed perpendicular to the long axis of the strand, Strand A will have the highest elastic modulus followed by Strand C with Strand B having the lowest compressive modulus (Wood Handbook 1999). Therefore, it was found that in the microscopic images of Strand B usually had

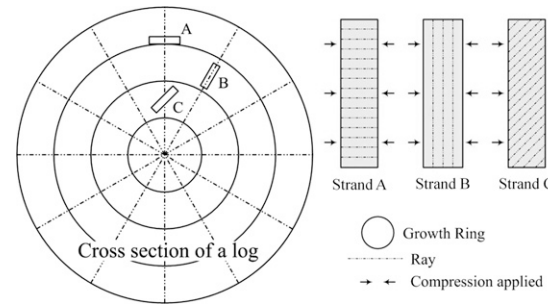

Figure 9. Variation of strand cutting orientation: Strand A was cut from longitudinal–tangential (LT) direction; Strand B was cut from longitudinal–radial (LR) direction; and Strand C was cut from a direction between LT and LR. The lines in the strands indicate the direction of rays.

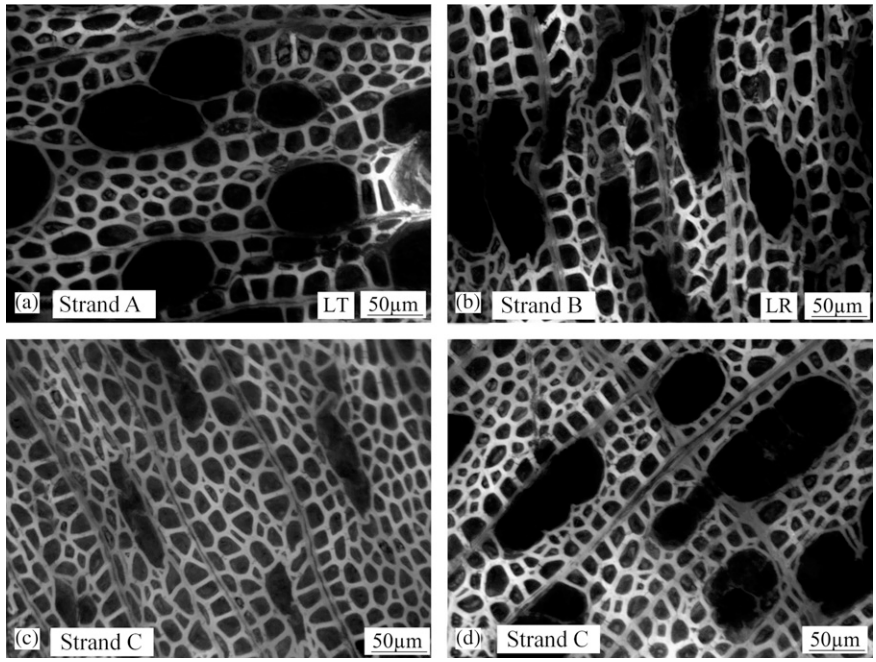

Figure 10. Orientations of strands as indicated in Figure 9 (a) Strand A cut in longitudinal–radial (LR) direction; (b) Strand B cut in longitudinal–tangential (LT) direction; (c) and (d) are Strand C cut between LR and LT directions.

the largest deformation among the three types.

3. Variability in the formation of the mat. Regardless of whether the mat is hand- or machine-formed, the result is that some columns in the transverse plane have more than the average strand counts and some less than average. This will lead to zones of higher and lower density in the finished panel and those zones will experience varying degrees of compression and associated structure damages.
4. Finally, there is the difference within the woody material itself. The growing environment, local climate, treatment conditions after logging, and the location and orientation of a strand in the stem all result in highly variable strand properties, especially the elastic modulus, which yields different behaviors under compression. Aspen is a relatively uniform density growth ring compared with other species and it is expected that the variability seen in this study would be larger for other species that have more pronounced differences between the earlywood and latewood and between cell lumens.

CONCLUSIONS

1. The method used to prepare slides for microscopic examination of OSL was able to retain the original condition of strands and voids through a full cross-section of board. It can also be applied to the examination of other types of wood composites.
2. The forming/deformation mechanism of interstrand voids could be tracked through progressively higher degrees of mat compression. The overlapping of strands created noncontact voids and partially filled edge voids that behaved differently during compression. Interstrand voids decreased in size and quantity with increasing board density, and above 625 kg/m^3, most interstrand voids were compressed to a smaller size than the vessels in the strands.
3. The collapse of cell lumens during the compression was due to the failure of cell

walls under axial loads or a combination of axial and lateral loads.

4. Generally vessels were compressed before any substantial deformation of fibers due to their larger diameters and thinner cell walls. There was significant variation in cell compression behavior both within and between strands in a board cross-section. This was attributed to differences in strand cutting orientation, heterogeneity of mat structure, and variation in wood properties of strands cut from different positions within the tree stems and variation between trees.

ACKNOWLEDGMENTS

The financial support from Forestry Innovation Investment Ltd. is greatly appreciated. A special thanks to Ainsworth Lumber Canada Ltd. for providing the strands, to Hexion Canada for the PF resin, and to Dr. Simon Ellis (Department of Wood Science, UBC) for the use of the facilities. Thanks were also extended to Dr. Kate Semple, Department of Wood Science, for comments on the manuscript.

REFERENCES

Blair S, Berge P, Berryman J (1996) Using two-point correlation functions to characterize microgeometry and estimate permeabilities of sandstones and porous glass. J Geophys Res 101(B9):20359-20376.

Bolton AJ, Humphrey PE (1994) The permeability of wood-based composite materials. Part 1. A review of the literature and some unpublished work. Holzforschung 48 (Suppl):95-100.

Dai C, Steiner PR (1993) Compression behavior of randomly-formed wood flake mats. Wood Fiber Sci 25(4):349-358.

Dai C, Yu C, Zhou X (2005) Heat and mass transfer in wood composite panels during hot pressing: Part II. Modeling void formation and mat permeability. Wood Fiber Sci 37(2):242-257.

Flannery BP, Deckman HW, Roberge WG, D'Amico KL (1987) Three-dimensional X-ray microtomography. Science 237(4821):1439-1444.

Geimer RL, Mahoney RJ, Loehnertz SP, Meyer RW (1985) Influence of processing-induced damage on strength of flakes and flakeboards. Paper 463. USDA Forest Products Laboratory, Madison, WI. 15 pp.

Jana D (2006) Sample preparation techniques in petrographic examination of construction materials: A state of the art review. Pages 23-70 *in* Proc 28th Conference on Cement Microscopy, 30 April-4 May 2006, Denver, CO.

Kostiainen K, Kaakinen S, Warsta E, Kubiske ME, Nelson ND, Sober J, Karnosky DF, Saranpaa P, Vapaavuori E (2008) Wood properties of trembling aspen and paper birch after 5 years of exposure to elevated concentrations of CO_2 and CO_3. Tree Physiol 28(5):805-813.

Kultikova EV (1999) Structure and properties relationships of densified wood. MS thesis, Virginia Polytechnic Institute and State University, Blacksburg, VA. 136 pp.

Lu S, Landis E, Keane D (2006) X-ray microtomographic studies of pore structure and permeability in Portland cement concrete. Mater Struct 39(6):611-620.

Müller U, Gindl W, Teischinger A (2003) Effects of cell anatomy on the plastic and elastic behavior of different wood species loaded perpendicular to grain. IAWA J 24(2): 117-128.

Panshin AJ, de Zeeuw C (1980) Textbook of wood technology. McGraw-Hill, New York, NY. 722 pp.

Schaap MG, Lebron I (2001) Using microscope observations of thin sections to estimate soil permeability with the Kozeny-Carman equation. J Hydrol 251(3-4): 186-201.

Siau JF (1995) Wood: Influence of moisture on physical properties. Dept. of Wood Science and Forest Products, Virginia Polytechnic Institute and State University, Blacksburg, VA. 227 pp.

Sugimori M, Lam F (1999) Macro-void distribution analysis in strand-based wood composites using an X-ray computer tomography technique. J Wood Sci 45(3): 254-257.

Tabarsa T, Chui YH (2000) Stress-strain response of wood under radial compression. Part I. Test method and influences of cellular properties. Wood Fiber Sci 32(2): 144-152.

Tabarsa T, Chui YH (2001) Characterizing microscopic behavior of wood under transverse compression. Part II. Effect of species and loading direction. Wood Fiber Sci 33(2):223-232.

Wood Handbook (1999) Wood as an engineering material. Gen Tech Rep FPL-GTR-113. USDA Forest Products Laboratory, Madison, WI. 463 pp.

Zhang B, Wu Q, Wang L, Han G (2005) Characterization of internal void structure of strand-based wood composites using X-ray tomography and digital tools. Pages 1-5 *in* Proc McMat2005—The 2005 joint ASME/ASCE/SES Conference on Mechanics and Materials, 1-3 June 2005, Baton Rouge, LA.

Zhang C (2009) Measurement and modeling of the in-plane permeability of oriented strand-based wood composites. MSc Thesis, University of British Columbia, Vancouver, BC. 89 pp.

Zhang C, Smith GD (2010) In-plane permeability of oriented strand lumber Part I: The effects of mat density and flow direction. Wood Fiber Sci 42(1):99-106.